

See discussions, stats, and author profiles for this publication at: <https://www.researchgate.net/publication/269933852>

# Mutant Poisoning Demonstrates a Nonsequential Mechanism for Digestion of Double-Stranded DNA by $\lambda$ Exonuclease Trimers

ARTICLE *in* BIOCHEMISTRY · DECEMBER 2014

Impact Factor: 3.02 · DOI: 10.1021/bi501431w · Source: PubMed

---

CITATIONS

2

---

READS

28

## 5 AUTHORS, INCLUDING:



Charles E Bell

The Ohio State University

40 PUBLICATIONS 1,552 CITATIONS

SEE PROFILE

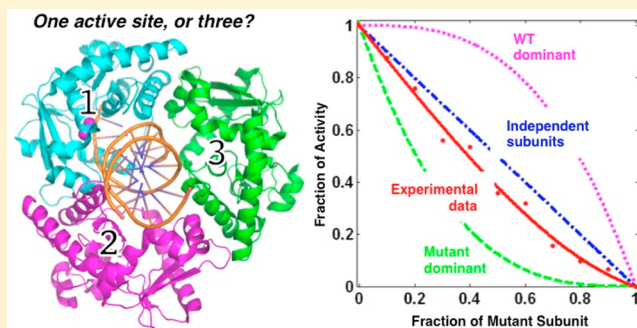
## Mutant Poisoning Demonstrates a Nonsequential Mechanism for Digestion of Double-Stranded DNA by $\lambda$ Exonuclease Trimers

Xinlei Pan,<sup>†,‡</sup> Jing Yan,<sup>§</sup> Aalapi Patel,<sup>‡</sup> Vicki H. Wysocki,<sup>†,§</sup> and Charles E. Bell\*,<sup>†,‡,§</sup>

<sup>†</sup>Ohio State Biochemistry Program, <sup>‡</sup>Department of Molecular and Cellular Biochemistry, and <sup>§</sup>Department of Chemistry and Biochemistry, The Ohio State University, Columbus, Ohio 43210, United States

Supporting Information

**ABSTRACT:**  $\lambda$  Exonuclease ( $\lambda$ exo) is a highly processive 5'-3' exonuclease that binds double-stranded DNA (dsDNA) ends and digests the 5'-strand into mononucleotides. The enzyme forms a toroidal homotrimer with a central tapered channel for tracking along the DNA. During catalysis, dsDNA enters the open end of the channel, and the 5'-strand is digested at one of the three active sites. It is currently not known if  $\lambda$ exo uses a sequential mechanism, in which the DNA moves from one active site to the next around the trimer for each round of catalysis or a nonsequential mechanism, in which the DNA locks onto a single active site for multiple rounds. To understand how  $\lambda$ exo uses its three active sites, we used a mutant poisoning approach, in which a 6xHis-tagged K131A inactive mutant of  $\lambda$ exo was mixed with untagged wild type (WT) to form hybrid trimers. Nickel-spin pull-down analysis confirmed complete subunit exchange after 1 h at 37 °C. Exonuclease assays revealed an approximately linear decrease in activity with increasing fraction of mutant, as expected for a nonsequential mechanism. By fitting the observed rates of digestion to a simple mathematical model, the individual rates of the two hybrid species of trimer were determined. This analysis showed that trimers containing only one or two WT subunits contribute significantly to the observed activity, in further agreement with a nonsequential mechanism. Finally, purification of hybrid trimer mixtures by Ni-spin chromatography, to remove the contribution from fully WT trimers, also resulted in significant levels of activity, again consistent with a nonsequential mechanism.



$\lambda$  Exonuclease ( $\lambda$ exo) ( $M_r$  25.9 kDa; 226 amino acids) is a component of the red recombination system of phage  $\lambda$ , which promotes homologous recombination by a simple single-strand annealing mechanism.<sup>1,2</sup> The enzyme binds to double-stranded DNA (dsDNA) ends and resects the 5'-strand to yield 5'-mononucleotides and a long 3'-ssDNA overhang.<sup>3,4</sup> The 3'-overhang is a substrate for an annealing reaction that is promoted by a second protein called Red $\beta$ .<sup>5</sup> Recombination generates end-to-end concatemers of the phage genome, which facilitates viral replication and packaging. Related "SynExo" recombination systems are found in a wide variety of bacteriophage and in dsDNA viruses that infect mammalian cells.<sup>6,7</sup> The two most well studied of these, the red system of phage  $\lambda$ , and RecET of the rac prophage of *Escherichia coli*,<sup>8</sup> have been exploited in powerful new methods for genetic engineering termed "recombineering".<sup>9–13</sup>  $\lambda$ exo is also being used in several other new biotechnology applications, such as Chip-Exo DNA footprinting,<sup>14</sup> nanopore DNA sequencing,<sup>15</sup> construction of genome libraries,<sup>16,17</sup> and in biosensors to detect specific sequences of DNA,<sup>18–21</sup> microRNA,<sup>22,23</sup> enzymes,<sup>24–26</sup> and small molecules.<sup>27,28</sup> Given the wide use of  $\lambda$ exo in these emerging technologies, there is a growing interest in understanding its mechanism of action.

The crystal structure of  $\lambda$ exo revealed a toroidal homotrimer with a central tapered channel for tracking along the DNA.<sup>29</sup>

The channel is wide enough at one end to accommodate dsDNA but narrows at the other end to only allow the passage of ssDNA. On the basis of this structure, a model was proposed in which the 3'-overhang threads through the central hole on the trimer as the enzyme tracks along the DNA digesting the 5'-strand. This model nicely accounts for the highly processive nature of the reaction, since the enzyme remains topologically linked to the DNA as it digests it. The monomer of  $\lambda$ exo adopts the type II restriction endonuclease-like fold that is found in numerous restriction enzymes and in several endo- and exonucleases involved in DNA repair and RNA processing.<sup>30,31</sup> These proteins all contain a conserved PD-(D/E)XK motif that contains two acidic residues for binding Mg<sup>2+</sup> and a lysine that is involved in activating the hydrolytic water molecule.<sup>32</sup>

The RecE protein of the RecET recombination system, which performs a similar function as  $\lambda$ exo but shares only limited sequence homology, forms a toroidal tetramer with a central channel of similar size and shape as that on the  $\lambda$ exo trimer.<sup>33</sup> Interestingly, although RecE and  $\lambda$ exo share a common core fold, the subunits pack into their respective oligomers in different orientations, suggesting that the two

**Received:** November 19, 2014

**Published:** December 22, 2014



ACS Publications

© 2014 American Chemical Society

proteins have evolved by separate paths, likely from a common ancestor that was monomeric, to form ring-shaped oligomers for processing dsDNA breaks. The conserved toroidal architecture of RecE and  $\lambda$ exo suggests an important role for the oligomeric ring in carrying out the function.

Crystal structures of  $\lambda$ exo in complex with DNA<sup>34</sup> confirmed the binding of DNA to the central channel as predicted but also revealed several unexpected features. The structure revealed that the enzyme unwinds exactly two base pairs from the 5'-end of the DNA prior to digestion, such that two nucleotides from the 5'-strand insert into the active site of one subunit of the trimer, while the 3'-strand pokes through the central channel to emerge out the back. Unwinding of the DNA is facilitated by a hydrophobic wedge on the protein that forms favorable interactions with the bases exposed at the junction. An arginine residue from one of the subunits of the trimer, Arg-45, inserts into the minor groove at the downstream end of the DNA, likely to act as a rudder to keep the enzyme on track as it moves along the DNA. The scissile phosphate on the 5'-strand bridges two active site Mg<sup>2+</sup> ions, and the terminal 5'-phosphate binds to a positively charged pocket at the end of the active site cleft.<sup>34,35</sup> On the basis of this structure, an “electrostatic ratchet” mechanism was proposed, in which the attraction of the 5'-phosphate generated after each round of cleavage to the positively charged pocket at the end of the active site helps to drive the enzyme forward along the DNA for each new round of cleavage.

For a ring-shaped oligomer such as  $\lambda$ exo, two fundamentally different types of mechanisms can be envisioned: a sequential mechanism, in which the DNA moves from one active site to the next around the oligomer for each new round of cleavage, or a nonsequential mechanism, in which the DNA locks onto a single active site on the oligomer for multiple rounds. Given that RecE and  $\lambda$ exo have both evolved to form toroidal oligomers with multiple active sites, one might expect the ring-shaped architecture to be actively used in the mechanism. Moreover, a sequential mechanism has been demonstrated for other ring-shaped oligomers, such as hexameric helicases<sup>36,37</sup> and F<sub>1</sub>-ATPase.<sup>38</sup> On the other hand, the electrostatic ratchet model described above, which is based on the crystal structures, predicts a nonsequential mechanism of action. A sequential mechanism seems overly complicated in that a large network of protein–DNA interactions would have to be broken at each cycle of the reaction, in order for the DNA to move from one active site to the next. Other ring-shaped oligomers that use a sequential mechanism bind and hydrolyze ATP, which drives large-scale conformational changes, such as subunit-reorientations and domain movements.  $\lambda$ exo does not bind or hydrolyze ATP, and although it could potentially use the energy of phosphodiester bond cleavage to drive translocation, large-scale conformational changes have not yet been observed in the different subunits of the trimer or in the different DNA-bound states.<sup>29,34</sup> Thus, we hypothesize that  $\lambda$ exo uses a nonsequential mechanism, but this has yet to be assessed experimentally.

In this work, we used a mutant poisoning approach, in which inactive mutant subunits were mixed with WT subunits to form hybrid trimers, to determine if  $\lambda$ exo uses a sequential or nonsequential mechanism for digestion of dsDNA substrates. In a sequential mechanism, the presence of one inactive subunit would be predicted to render a trimer inactive, such that a dramatic decrease in total activity would be expected with increasing fraction of mutant. By contrast, in a nonsequential mechanism, in which trimers containing mutant subunits are

still active, the decrease in activity would be expected to be more linear. Measurements of the rates of dsDNA digestion revealed an approximately linear decrease in activity with increasing fraction of mutant. Thus, the experimental data are consistent with a nonsequential mechanism.

## EXPERIMENTAL PROCEDURES

**Protein Expression and Purification.** WT and K131A versions of  $\lambda$ exo were expressed and purified as has been described.<sup>34</sup> Briefly, the proteins were expressed from a pET14b vector as N-terminal 6xHis-tag fusions in *E. coli* BL21-AI cells and purified by Ni-affinity chromatography. A portion of each protein was subjected to thrombin cleavage to remove the 6xHis-tag, and any residual uncleaved protein was removed by a reverse nickel column. For the remaining portions of the WT and K131A proteins, the 6xHis tags were left intact. All proteins were further purified by anion exchange chromatography on Hi-Trap QFF (GE Healthcare), dialyzed into 20 mM Tris (pH 7.5), 1 mM dithiothreitol, concentrated to ~15 mg/mL, and stored at -80 °C in small aliquots. Protein concentrations were determined by absorbance at 280 nm using the extinction coefficient calculated from the amino acid sequence, which was 46 410 M<sup>-1</sup> cm<sup>-1</sup> (per monomer) for all proteins. All protein concentrations are given in the text as moles of trimer.

**Nickel-Spin Pull-down Assay.** A nickel-spin pull-down assay was used to monitor exchange of subunits between trimers of 6xHis-K131A (28.0 kDa) and untagged WT (26.2 kDa)  $\lambda$ exo proteins. The two proteins were mixed at 10  $\mu$ M total trimer (5  $\mu$ M each) in Buffer A (50 mM NaH<sub>2</sub>PO<sub>4</sub>, 300 mM NaCl, 10 mM imidazole, pH 8.0) and incubated for varying times and temperatures to allow for subunit exchange. Protein mixtures (100  $\mu$ L) were loaded onto a Ni-NTA Spin column (Qiagen) that was pre-equilibrated with Buffer A and washed three times (200 or 600  $\mu$ L each, as specified) with Buffer A with 30 mM imidazole. Bound proteins were eluted from the column with 100  $\mu$ L of Buffer A with 500 mM imidazole. All fractions were analyzed by 13.5% SDS-PAGE with Coomassie Blue stain.

**Exonuclease Assay.** To quantify exonuclease activity, digestion of a 2686 bp, *Pst*I-linearized pUC19 DNA substrate (NEB) was monitored by agarose gel electrophoresis. The assay was performed with a 2–33-fold excess of DNA substrate over enzyme, as specified for each experiment in the figure legends. Under these conditions, one strand of the dsDNA substrate is digested completely to release mononucleotides and the intact (opposing) strand of ssDNA as products. The linear pUC19 DNA was <sup>32</sup>P 3'-end-labeled with terminal transferase (NEB) in 50  $\mu$ L reactions containing 1× TdT buffer (NEB), 0.25 mM CoCl<sub>2</sub>, 5.0 pmol of pUC19 DNA (10 pmol of DNA ends), 20 pmol of  $\alpha$ -<sup>32</sup>P-ddATP (PerkinElmer) and 10 units of terminal transferase. The reaction was incubated at 37 °C for 30 min and quenched by adding 10  $\mu$ L of 0.2 M EDTA (pH 8.0). Labeled DNA was separated from other reaction components by gel filtration on G-25 MicroSpin columns (GE Healthcare).

Exonuclease reactions contained 67 mM glycine-KOH (pH 9.4), 2.5 mM MgCl<sub>2</sub>, 50  $\mu$ g/mL BSA, and 1 nM <sup>32</sup>P 3'-end-labeled pUC19 DNA substrate. The above components were incubated at 37 °C for 10 min before adding 0.03–0.5 nM  $\lambda$ exo (as indicated) to initiate the reaction. At each time point, a 10  $\mu$ L aliquot was removed from the reaction, quenched by adding 1  $\mu$ L of 250 mM EDTA and 2  $\mu$ L of BlueJuice loading dyes (Invitrogen), and analyzed by electrophoresis on 0.8% agarose

gels in TAE buffer. The gels were dried and autoradiographed using a Storm phosphorimager (GE Healthcare). Band intensities were quantified using ImageQuant software. The percentage of pUC19 DNA digested at each time point was calculated as

$$\% \text{digested} = \frac{I_s \times 2}{I_s \times 2 + I_D} \times 100\% \quad (1)$$

where  $I_D$  is the intensity of the band for dsDNA substrate, and  $I_s$  is the intensity of the band for ssDNA product.  $I_s$  was multiplied by 2 to account for the fact that the ssDNA product, which has one 3'-end, has half the radioactivity of the dsDNA substrate, which has two. The % digested was plotted versus time, and the initial, linear portion of the curve was fit to determine the slope. The rate of digestion, in nucleotides/second per trimer, was calculated as

$$\text{rate} = \frac{\text{slope} \times n_{\text{pUC19}} \times 2686}{n_{\text{Exo}} \times 60} \quad (2)$$

where  $n_{\text{pUC19}}$  is the number of molecules of pUC19 dsDNA substrate,  $n_{\text{Exo}}$  is the number of  $\lambda$ exo trimers, and 2686 is the number of base pairs in pUC19.

**Gel Shift DNA-Binding Assay.** A gel-shift assay was used to compare the binding of K131A and WT  $\lambda$ exo to a 12-mer DNA duplex that contained a 2-nucleotide 5'-overhang on one end. This was the same DNA that was used to determine the crystal structure of the complex.<sup>34</sup> The DNA was  $^{32}\text{P}$  5'-end-labeled with T4 polynucleotide kinase (NEB). Each 20  $\mu\text{L}$  labeling reaction contained 20 pmol of the 14-mer oligonucleotide, 20 pmol of  $\gamma$ - $^{32}\text{P}$ -ATP (PerkinElmer), and 20 units of T4 PNK enzyme in the NEB reaction buffer. Reactions were incubated for 30 min at 37 °C and purified by gel filtration on a G-25 MicroSpin column (GE Healthcare). The  $^{32}\text{P}$  5'-end-labeled 14-mer oligonucleotide was then annealed to a complementary 12-mer strand by incubating for 10 min at 95 °C and cooling slowly to room temperature to allow for annealing. Each 10  $\mu\text{L}$  binding reaction contained varying concentrations of  $\lambda$ exo (80–1000 nM), 1  $\mu\text{L}$  of 50 000 cpm DNA substrate (approximately 3 nM molecules), 20 mM Tris (pH 7.5), 10 mM CaCl<sub>2</sub>, and 1 mM DTT. Reactions were incubated at 25 °C for 10 min, mixed with 3  $\mu\text{L}$  of loading dyes (20% glycerol, 0.12% bromophenol blue, and 0.12% xylene cyanol), and analyzed by native PAGE in TBE buffer. Gels were dried and autoradiographed using a Storm phosphorimager (GE Healthcare).

**Mass Spectrometry.** The untagged K131A, 6xHis-WT, and a 1:1 mixture of untagged K131A and 6xHis-WT were buffer exchanged at 100  $\mu\text{M}$  into 100 mM ammonium acetate using Micro Bio-Spin 6 columns (Bio-Rad). Nanoelectrospray ionization mass spectrometry (nano-ESI-MS) analysis was performed on a modified Synapt G2-S HDMS mass spectrometer (Waters Corp., Manchester, U.K.) with a customized surface-induced dissociation (SID) device installed before the ion mobility cell as described previously.<sup>39</sup> Each sample was filled into a glass capillary pulled using a Sutter Instruments P-97 micropipette puller (Novato, CA) and ionized with a nanoelectrospray source at a voltage of 1.0–1.5 kV. The sampling cone voltage was set to 20 V, and the source offset voltage was set to 20 V. Other instrument conditions were 2.6 mbar for the backing pressure,  $5 \times 10^{-3}$  mbar for the source pressure, 120 mL/min gas flow to the helium cell, 60 mL/min gas flow to the ion mobility cell, and 7

$\times 10^{-7}$  mbar in the time-of-flight (TOF) analyzer. Each peak present in the mass spectra was subsequently selected and further dissociated in SID with an acceleration voltage of 50 V. This value multiplied by the charge state provides the collision energy in eV.

## RESULTS

**Experimental Approach.** Constructs containing “concatemers” of fused subunits have proven informative for probing the mechanisms of other ring-shaped oligomers, such as ClpX protease,<sup>40</sup> GroEL,<sup>41</sup> and GroES.<sup>42</sup> When the individual subunits are linked together in a single, continuous polypeptide, mutations can be introduced to selectively inactivate specific subunits within the oligomer, and the activity of a single species can be measured. However, in the case of  $\lambda$ exo, the C-terminus of a given subunit is 56 Å from the N-terminus of one neighboring subunit and 71 Å from the other (Figure S1, Supporting Information), making it difficult to design appropriate linkers. We therefore turned to a “mutant poisoning” approach, in which inactive mutant subunits are mixed with WT subunits to form hybrid trimers. Under conditions that promote efficient exchange of subunits, a distribution of different hybrid oligomers will form, and the observed activity will be the sum of the contributions of the individual components. With appropriate data analysis, this method has been used to provide valuable mechanistic information on other ring-shaped oligomeric proteins, such as T7 DNA helicase<sup>37</sup> and F<sub>1</sub>-ATPase.<sup>38</sup>

**Quantitative Exonuclease Assay.** In a previous study, we monitored  $\lambda$ exo activity on a linear 2.7 kb pUC19 dsDNA substrate by agarose gel electrophoresis with SyBr Gold staining.<sup>34</sup> Under conditions of limiting enzyme (>20-fold excess of dsDNA over  $\lambda$ exo trimers), this assay simultaneously shows depletion of dsDNA substrate and accumulation of ssDNA product and thus nicely demonstrates the processive nature of the reaction. However, this assay was not quantitative because the observed intensity of SyBr Gold fluorescence did not vary linearly with DNA concentration. We therefore used a similar assay but with  $^{32}\text{P}$  end-labeled dsDNA substrate. Since  $\lambda$ exo digests mononucleotides from the 5'-end of dsDNA, we used dsDNA that was labeled with  $^{32}\text{P}$  at the 3'-end. We first verified that the intensity of bands for dsDNA and ssDNA, as measured by phosphorimaging, varied linearly with DNA concentration. This was indeed the case, as shown for dsDNA substrate in Figure S2, Supporting Information. An agarose gel monitoring the reaction of 1.2 nM dsDNA with 0.05 nM  $\lambda$ exo trimer is shown in Figure 1A. The rate of digestion was determined from a time course of % DNA digested (Figure 1B), as described in Experimental Procedures. For WT  $\lambda$ exo the rate determined by this method was  $44 \pm 9$  nucleotides/s per trimer, based on three independent measurements. This is in general agreement with rates ranging from 3 to 32 nucleotides/s determined either biochemically<sup>3,35,43</sup> or in four different single-molecule studies.<sup>44–47</sup> In other single-molecule studies, significantly higher rates (~1000 nucleotides/s) have been reported, for reasons that are not yet clear.<sup>48–52</sup>

**The K131A Mutant of  $\lambda$ exo Is Suitable for Mutant Poisoning.** Lys-131 is the conserved, active-site lysine of the PD-(D/E)XK motif of  $\lambda$ exo. The K131A mutant was previously used to trap a stable DNA complex for crystallographic analysis,<sup>34</sup> indicating that the protein is completely inactive. Indeed, we observed no activity at all for the K131A protein with our  $^{32}\text{P}$  3'-end-labeled dsDNA substrate (Figure 2A). To

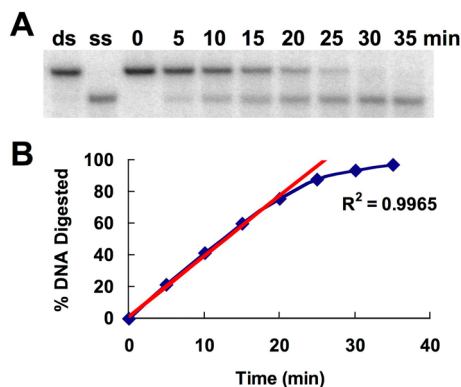


**Figure 1.** Exonuclease assay. (A) Agarose gel showing a time course for the reaction of 0.05 nM WT  $\lambda$ exo trimer with 1.2 nM of  $^{32}$ P 3'-end-labeled linear 2686 bp pUC19 dsDNA. The upper band is the dsDNA substrate, and the lower band is the ssDNA product. The lanes labeled “ds” and “ss” show control reactions without enzyme. The “ss” lane contains half the normal amount of dsDNA heated for 5 min at 95 °C to mimic the band expected for ssDNA product. (B) Plot of % DNA digested vs time for the reaction of panel A. The %DNA digested was calculated from the intensities of the bands for substrate and product, as described in Experimental Procedures. The red line shows the fit of the data in the linear portion of the reaction, from which a rate of 41 nt/second was calculated. The average rate from three independent measurements was  $44 \pm 9$  nt/s.

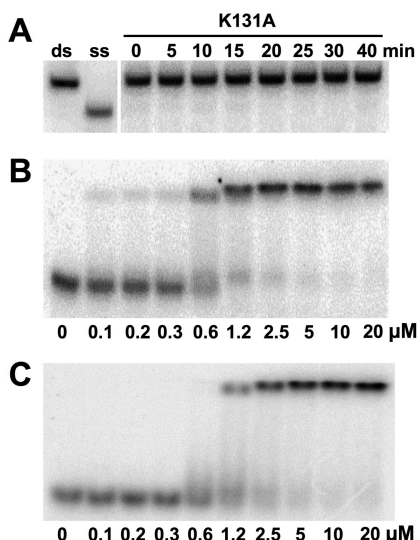


**Figure 2.** K131A mutant of  $\lambda$ exo binds DNA but is completely inactive for cleavage. (A) Agarose gel showing the reaction of 0.05 nM K131A trimer with 1 nM  $^{32}$ P 3'-end labeled linear pUC19 dsDNA substrate. Notice that the K131A protein is completely inactive (no ssDNA product is formed). (B, C) Gel shift shows binding of WT (B) or K131A (C)  $\lambda$ exo to 3 nM  $^{32}$ P 5'-end labeled 14-mer/12-mer dsDNA substrate. The numbers below each lane give the concentration of  $\lambda$ exo trimer in the binding reaction. Notice that the K131A protein binds to the DNA with similar affinity as WT.

measure the ability of the K131A protein to bind DNA, we used a gel-shift assay with a short  $^{32}$ P 5'-end-labeled dsDNA substrate (Figure 2B,C). This experiment shows that the K131A protein has only slightly reduced DNA-binding affinity compared to WT. Thus, the mutation does not interfere with the folding of the protein or the assembly of trimers. These results demonstrate that the K131A protein is suitable for the mutant poisoning experiments.

**Direct Addition of K131A Does Not Affect the Activity of WT  $\lambda$ exo.** We first determined if the K131A protein affected the activity of WT  $\lambda$ exo when the two were added at the same time to initiate a reaction. Figure 3 shows the time courses for

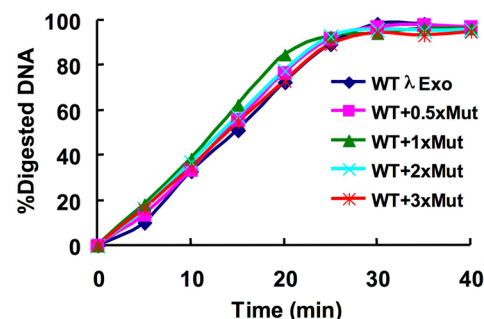


**Figure 3.** Exonuclease activity of WT  $\lambda$ exo in the presence of increasing amounts of the K131A mutant. The reactions were performed as described in Figure 1, except that 1 nM of dsDNA substrate was used, and the indicated amount of K131A mutant was added immediately prior to initiating the reaction by addition of a fixed amount of WT (0.03 nM trimer). Notice that the addition of even a 3-fold excess of K131A mutant has no effect on the activity observed for WT.

reactions in which increasing amounts of K131A were added to a fixed amount of WT, in the presence of a 33-fold molar excess of dsDNA. As seen in the figure, the addition of even a 3-fold excess of the K131A protein has no observable effect on the activity of WT  $\lambda$ exo. We infer from this observation that either the K131A subunits are not exchanging into the WT trimers, or that subunit-exchange is taking place, but the presence of mutant subunits does not reduce the activity of the WT subunits. Since all of the molecules of substrate are converted to product, it can be inferred from this experiment that the K131A trimers (or subunits) do not block WT trimers from accessing the dsDNA ends. Although K131A trimers bind efficiently to DNA ends as shown in Figure 2C, apparently they exchange on and off the DNA rapidly enough to allow access of WT trimers. Once a WT trimer binds, it presumably begins digesting and moving forward along the DNA processively, such that it can no longer be blocked by a K131A trimer.

**Subunit Exchange Occurs Readily at 37 °C in the Absence of DNA.** To determine if subunits can be exchanged between 6xHis-K131A and untagged WT  $\lambda$ exo trimers, a Ni-spin pull-down assay was performed with purified proteins. The tagged and untagged proteins differ in size by 1.9 kDa (17 amino acid residues) and can be resolved into distinct bands by SDS-PAGE. Figure 4A shows a control experiment in which 100  $\mu$ L of 10  $\mu$ M 6xHis-K131A and WT proteins were loaded onto separate Ni-spin columns. Under the experimental conditions, all of the 6xHis-K131A protein bound to the column and required high imidazole (500 mM) for elution. By contrast, none of the untagged WT protein bound to the column: most of it eluted in the flow through at 10 mM imidazole, and the rest eluted in the wash (W1) at 30 mM imidazole. These results establish that the Ni-spin procedure can be used to monitor subunit exchange.

Next, equal amounts of 6xHis-K131A and untagged WT  $\lambda$ exo (5  $\mu$ M trimer of each) were incubated at different times and temperatures, and subjected to Ni-spin purification. If subunit exchange occurs during the incubation, hybrid trimers containing tagged and untagged subunits will be formed, and

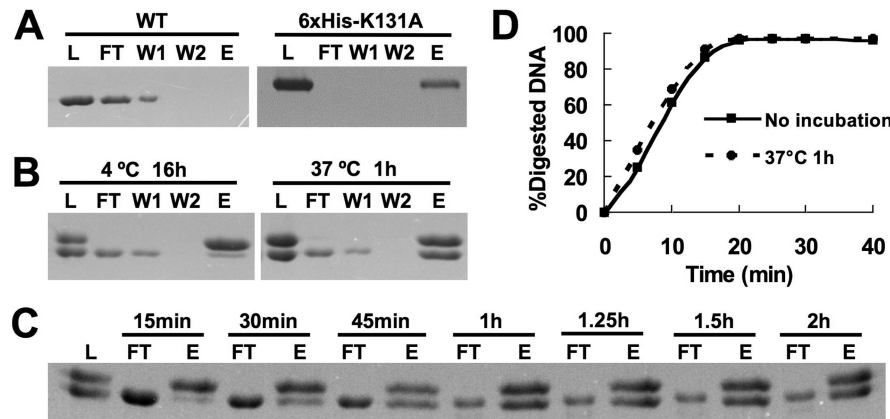


**Figure 4.** Nickel-spin pull-down assay to demonstrate subunit exchange. (A) Control experiments show that untagged WT  $\lambda$ exo does not bind to the Ni-spin column at all, while the 6xHis-K131A protein binds completely. A total of 100  $\mu$ L of 10  $\mu$ M untagged WT  $\lambda$ exo (left) or 6xHis-K131A (right) was loaded onto separate Ni-NTA spin columns, washed with 3  $\times$  200  $\mu$ L of 30 mM imidazole, and eluted with 500 mM imidazole, as described in Experimental Procedures. Ten microliters of each fraction was analyzed by SDS-PAGE with Coomassie Blue stain. (B) Similar experiments as panel A, except that equal amounts (5  $\mu$ M) of WT and 6xHis-K131A were incubated for 16 h at 4 °C (left) or 1 h at 37 °C (right), prior to loading onto the Ni-spin column. Notice that subunit exchange is detectable but not complete at 4 °C, and complete at 37 °C, since approximately equal amounts of the two proteins are present in the elution (lane E). (C) Elutions from experiments at increasing times of incubation at 37 °C demonstrate that subunit exchange reaches equilibrium within 1 h. (D) Exonuclease reactions with WT  $\lambda$ exo demonstrate that the 1 h incubation at 37 °C does not result in any loss of activity.

6xHis-K131A subunits will pull down untagged WT subunits. If there is no subunit exchange, only the 6xHis-K131A subunits will bind to the column and be eluted. The results show that for an overnight incubation at 4 °C, a small amount of untagged WT is retained on the column, and eluted with the 6xHis-K131A protein (Figure 4B). This indicates that subunit exchange does occur at 4 °C, but only very slowly. By contrast, for a 1 h incubation at 37 °C, approximately equal amounts of untagged WT and 6xHis-K131A eluted from the column, indicating that subunit exchange was complete. To determine the time it takes for subunit exchange to reach equilibrium, 6xHis-K131A and untagged WT were incubated at 37 °C for times ranging from 15 to 120 min prior to loading onto the Ni-spin column. The results show that subunit exchange reaches equilibrium within 1 h at 37 °C (Figure 4C).

It is conceivable that the retention of untagged WT subunits on the Ni-spin column is due to a trimer–trimer interaction or nonspecific aggregation that is induced by the 37 °C incubation, as opposed to formation of hybrid trimers. To observe formation of hybrid trimers directly, mixtures of untagged K131A and 6xHis-WT protein were incubated at 37 °C for 1 h, exchanged into 100 mM ammonium acetate (pH 6.8), and analyzed by native nanoelectrospray mass spectrometry (Figure 5). The 6xHis tag was moved to the WT protein for this experiment because the 6xHis-K131A protein was poorly soluble in the ammonium acetate buffer required for nanonelectrospray ionization. The 6xHis-WT was also poorly soluble in ammonium acetate but to a lesser extent than 6xHis-K131A. The resulting native mass spectrum shows clear peaks for the expected species of hybrid trimers (Figure 5). The species shown in Figure 5 were all further validated by MS/MS with surface induced dissociation used as the activation method. A representative tandem mass spectrum showing the SID of the 16+ WT<sub>1</sub>MUT<sub>2</sub> trimer (the highest peak in Figure 5C) is shown in Figure S3, Supporting Information. Because of the partial depletion of the 6xHis-WT protein in the ammonium acetate buffer, the intensities of peaks for the different species of hybrid trimer were not quantitative. Nonetheless, this experi-

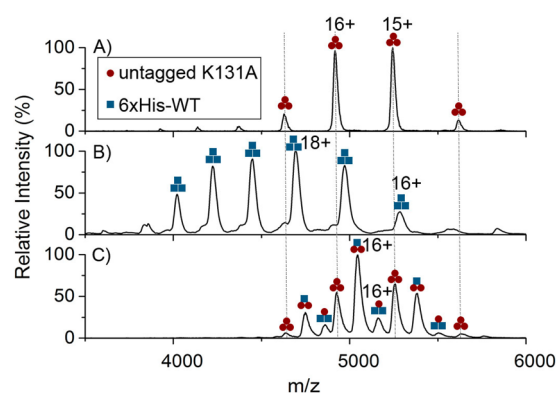


**Figure 5.** Native nanoelectrospray mass spectra of hybrid  $\lambda$ exo trimers. 100  $\mu$ M of protein was exchanged into 100 mM ammonium acetate (pH 6.8) using a Micro Bio-Spin 6 column and injected into a modified Synapt G2-S HDMS mass spectrometer. (A, B) Spectra for untagged K131A mutant (A) and 6xHis-WT (B) show the expected peaks for trimers. (C) Spectrum for a mixture of untagged K131A and 6xHis-WT shows the expected peaks for hybrid trimers, as indicated by the symbols (please refer to the key in panel A). Note that due to the partial precipitation of the 6xHis-WT protein (but not the untagged K131A protein) in the ammonium acetate buffer required for nanoelectrospray, the intensities of peaks for species containing 6xHis-WT subunits were lower than expected.

ment confirms that the expected species of hybrid trimer are being formed, as indicated by Ni-spin pull-down. It should be noted that no precipitation of the 6xHis-tagged protein was observed in the buffers used for the subunit-exchange experiments or the exonuclease assay. Moreover, the 6xHis tag does not affect the exonuclease activity of the WT enzyme.<sup>34</sup>

**Incubation for 1 h at 37 °C Does Not Affect Activity of WT  $\lambda$ exo.** The above results indicate that the efficient subunit-exchange necessary for the mutant poisoning approach can be achieved by incubation for 1 h at 37 °C. A potential concern, however, is that the heat treatment could reduce the activity of WT  $\lambda$ exo, which would complicate quantitative comparison of

subsequent rate measurements. Figure 4D shows the reaction time courses for WT  $\lambda$ exo that was incubated in buffer A at 37 °C for 1 h prior to adding to a reaction with DNA substrate, compared to enzyme that was added to the reaction directly from frozen stock thawed on ice, without heat treatment. The results show that the heat treatment has no effect on the observed activity.

**Mutant Poisoning Demonstrates a Nonsequential Mechanism for  $\lambda$ exo.** With a method to allow for efficient subunit exchange established, we proceeded to measure the exonuclease activity as a function of the fraction of K131A mutant present (Figure 6). In these experiments, the total

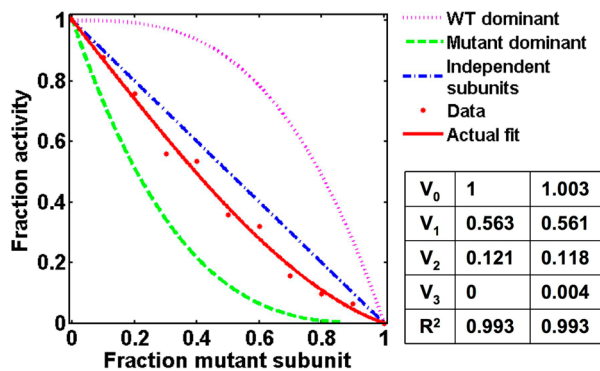


**Figure 6.** Mutant poisoning demonstrates a nonsequential mechanism for  $\lambda$ exo. The red data points show the experimentally determined cleavage rates, expressed as the fractional activity relative to WT, for mixtures of WT and K131A  $\lambda$ exo that were incubated for 1 h at 37 °C to allow subunit exchange. The total concentration of  $\lambda$ exo was fixed at 0.05 nM trimer, while the ratio of WT to K131A mutant was varied. The data points at higher fraction of mutant (0.6 to 0.9) used a higher amount of total enzyme, so that the slower rates could be determined accurately. The rates were determined as described in Experimental Procedures and shown in Figure 1 for WT. The solid red line shows a fit of the experimental data to eq 3 using MATLAB. The broken lines show the theoretical curves generated for three different models for the mechanism, as described in the text. The table shows the fractional activity of the different trimer species, determined from a fit of the data to eq 3. In the middle column, the values of  $V_0$  and  $V_3$  were fixed at 1 and 0 respectively. In the right column, all four values were allowed to vary, to show the stability of the fit. Notice that the experimental data are most consistent with a nonsequential mechanism (independent subunits model).

amount of  $\lambda$ exo protein (WT or K131A) was held fixed (at 0.05 nM trimer for most data points), while the fraction of the K131A mutant was increased by increments of 0.1. For the reactions at a fraction of mutant of 0.6–0.9, a higher amount of total enzyme was used, so that the slower rate could be measured accurately. However, the rate calculation corrects for the amount of enzyme present. Protein mixtures were incubated for 1 h at 37 °C to allow for subunit exchange, and a portion of the mixture was added to dsDNA substrate to initiate the reaction. Since the protein mixtures in this experiment were not subjected to Ni-spin purification, all species of trimer, including those with three WT subunits, were present in the reaction. The rates of digestion for each sample, expressed as the fraction of activity relative to WT, were determined by the agarose gel assay, as demonstrated in Figure 1 for WT. The results show an approximately linear decrease in activity with increasing fraction of K131A mutant (Figure 6). Qualitatively, the data are consistent with a nonsequential

mechanism, since in a sequential mechanism we would expect a much steeper, nonlinear decrease in activity with increasing fraction of K131A mutant.<sup>37</sup>

To obtain quantitative information from the data plotted in Figure 6, we developed a simple mathematical model to calculate the fractional amounts of each of the four possible species of trimer that should be present as a function of the fraction of K131A mutant. This model assumes that subunit exchange has fully equilibrated, as indicated by Ni-spin pull-down in Figure 4C. Briefly, if the fraction of mutant subunits is  $x$ , then the fraction of  $WT_3$  trimers is  $(1 - x)^3$ , the fraction of  $WT_2MUT_1$  trimers is  $3(1 - x)^2x$ , the fraction of  $WT_1MUT_2$  trimers is  $3(1 - x)x^2$ , and the fraction of  $MUT_3$  trimers is  $x^3$ . If we define the rate of digestion for  $WT_3$  trimers as  $V_0$ , the rate for  $WT_2MUT_1$  trimers as  $V_1$ , the rate for  $WT_1MUT_2$  trimers as  $V_2$ , and the rate for  $MUT_3$  trimers as  $V_3$ , then the total activity expected for the mixture can be expressed as

$$V = V_0(1 - x)^3 + 3V_1(1 - x)^2x + 3V_2(1 - x)x^2 + V_3x^3 \quad (3)$$

This equation was used to generate theoretical curves for the expected activity as a function of the fraction of mutant ( $x$ ), based on three different models for the mechanism. The green curve shows the activity expected for a “mutant dominant” model in which any trimer containing a mutant subunit is completely inactive, such that  $V_1 = V_2 = V_3 = 0$ , and  $V = V_0(1 - x)^3$ . This is the curve expected for a strictly sequential mechanism. The magenta curve shows the activity expected for a “WT dominant” model, in which any trimer that contains a WT subunit has the full activity of the  $WT_3$  trimer, such that  $V_1 = V_2 = V_0$ , and  $V_3 = 0$ . The blue curve shows the activity expected for an “independent subunits” model, in which the activity of a trimer is proportional to its fraction of WT subunits, such that  $V_1 = 2/3V_0$ ,  $V_2 = 1/3V_0$ , and  $V_3 = 0$ . In this model the subunits behave as if they were monomeric. Comparison of the experimental data (red data points) to the theoretical curves shows that the data are most consistent with the independent subunits model. The measured rates are however slightly and systematically lower than expected for this model. The possible reasons for this will be discussed below.

By fitting the experimental data for the observed rates of digestion at each fraction ( $x$ ) of K131A mutant to eq 3, values for  $V_1$  and  $V_2$  were determined, while fixing the values for  $V_0$  and  $V_3$  at 1 and 0, respectively, as shown to the right of the plot in Figure 6 (middle column). The solid red line on the plot shows the fit of the experimental data to the equation. The fitted values of 0.56 for  $V_1$  and 0.12 for  $V_2$  are close to, but slightly less than, the respective values of 0.67 and 0.33 expected for the independent subunits model. To assess the stability of the fit, the values of  $V_0$  and  $V_3$ , which are expected to be 1 and 0, were also allowed to vary. As shown in the right column of Figure 6, this did not change the values for any of the four fitted parameters significantly. This indicates that the fit is stable.

**Activity of Mixtures of  $\lambda$ exo Trimers Containing at Least One Mutant Subunit.** The experiments described above used protein mixtures that were not subjected to Ni-spin purification and therefore contained at least some percentage of  $WT_3$  trimers. As a further test of the nonsequential mechanism, we next measured the activity of hybrid trimer mixtures that were subjected to Ni-spin purification, to remove the contribution from  $WT_3$  trimers (Figure 7). The experiment was performed in two ways. First, to enrich for  $WT_2MUT_1$

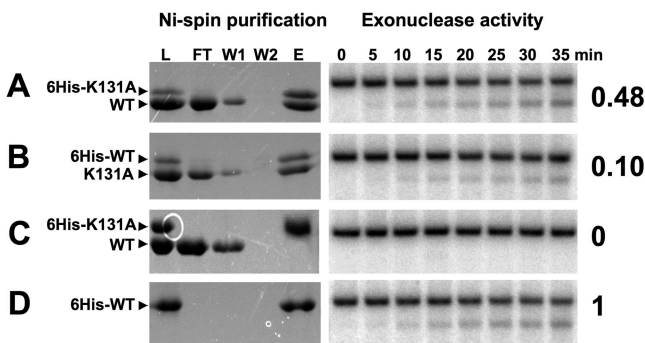


**Figure 7.** Trimers of  $\lambda$ exo containing at least one K131A mutant subunit are active. The SDS-PAGE gels on the left show Ni-spin purification of different mixtures of WT and K131A versions of  $\lambda$ exo. The agarose gels on the right show the exonuclease activity of the protein eluted from the column on the left. (A) 6xHis-K131A was mixed with an excess of untagged WT, heated for 1 h at 37 °C, and Ni-spin purified to enrich for WT<sub>2</sub>MUT<sub>1</sub> trimers. (B) 6xHis-WT was mixed with an excess of untagged K131A, heated for 1 h at 37 °C, and Ni-spin purified to enrich for WT<sub>1</sub>MUT<sub>2</sub> trimers. (C) Control in which 6xHis-K131 and untagged WT trimers were incubated separately for 1 h at 37 °C and then loaded sequentially onto the same Ni-spin column. None of the WT protein is present in the elution, and the eluted protein shows no activity. (D) Control in which 6xHis-WT protein was Ni-spin purified and used in a reaction to establish the level of activity expected for WT<sub>3</sub> trimers. The exonuclease reactions in panels A–D contained 0.2, 0.5, 0.5, and 0.1 nM of total  $\lambda$ exo trimer, respectively. The numbers to the right of each reaction give the fractional activities relative to the reaction with WT<sub>3</sub> trimers of panel D.

trimers (Figure 7A), 6xHis-K131A was mixed with an excess of untagged WT, incubated for 1 h at 37 °C to equilibrate subunit exchange, and subjected to Ni-spin purification. To prevent further subunit exchange, the eluted protein was placed immediately on ice and promptly used in the exonuclease assay. As shown in the left and right panels of Figure 7a, there is indeed an excess of untagged (WT) subunits present in the elution, and the eluted protein is active. In the second experiment, to enrich for WT<sub>1</sub>MUT<sub>2</sub> trimers, 6xHis-WT protein was mixed with an excess of untagged K131A, incubated for 1 h at 37 °C, and subjected to Ni-spin purification (Figure 7b). Again, an excess of untagged (K131A) protein was present in the elution, and the protein in the elution was active. These results demonstrate that  $\lambda$ exo trimers that contain at least one mutant subunit are active, as expected for a nonsequential mechanism.

To quantify the results, two control experiments were performed (Figures 7C,D). First, equal amounts of WT and 6xHis-K131A proteins were added sequentially to the same Ni-spin column, without prior mixing, and the column was washed and eluted as described above. SDS-PAGE analysis (Figure 7C, left) shows that all of the 6xHis-K131A protein, and none of the WT protein, was present in the elution (lane E). Moreover, the protein from the elution gave no detectable activity in the exonuclease assay (Figure 7C, right). This demonstrates that there is no subunit exchange on the column and that the washing procedure completely removes all WT<sub>3</sub> trimers, so that none are present in the elution. Second, to establish the level of activity expected for WT<sub>3</sub> trimers under these conditions, the N-spin procedure was used to purify 6xHis-WT protein, which was then added to a reaction (Figure 7D). This control was necessary because the Ni-spin procedure reduces the activity of

the protein, from 44 ± 9 to 10.3 ± 2.5 nt/s/trimer, for unknown reasons.

The values to the right of Figure 7 give the exonuclease activities for each of the four different trimer preparations, expressed as the fraction of activity relative to that measured for Ni-spin purified WT<sub>3</sub> trimers (panel D). Note that different amounts of each eluted protein were added to the exonuclease reactions shown on the right, so that the rates could be measured accurately. Thus, to compare the activities of the different trimer preparations, one should compare the values for the fractional activities shown at right, which take into account the amount of enzyme added, as opposed to the amount of product seen in the gels. The value of 0.48 for the preparation of WT<sub>2</sub>MUT<sub>1</sub> trimers (Figure 7A) is close to the value of 0.56 determined for V<sub>1</sub> from the fit to the data in Figure 6. Similarly, the value of 0.10 for WT<sub>2</sub>MUT<sub>1</sub> trimers is close to the value of 0.12 determined in Figure 6 for V<sub>2</sub>. In summary, these results demonstrate that trimers containing at least one mutant subunit are active, as expected for a nonsequential mechanism. Moreover, the agreement between the values for V<sub>1</sub> and V<sub>2</sub> obtained in the different experiments of Figures 6 and 7 suggests that the quantitative comparisons are valid.

One could argue that the activity observed in this experiment is due to WT<sub>3</sub> trimers that form as a result of subunit exchange that happens *after* the Ni-spin procedure, either during the ~30 min that the protein was incubated on ice before being added to the exonuclease reaction, or during the exonuclease reaction itself, which was performed at 37 °C. As shown by the Ni-spin experiments in Figure 4B, subunit exchange occurs exceedingly slowly at 4 °C, such that the first possibility is unlikely. Although subunit-exchange does occur at 37 °C, as shown in Figure 4B,C, the experiments of Figure 3 show that a 3-fold excess of K131A protein added at the beginning of the exonuclease reaction does not affect the activity of WT protein. This suggests that subunit-exchange does not occur during the exonuclease reaction itself, even though the assay was performed at 37 °C. It is likely that the  $\lambda$ exo trimers are more stable, and thus less prone to subunit exchange, when they are bound to and actively working on a DNA substrate, which was present in >33-fold excess at the beginning of the reaction. Even if we assume that subunit-exchange did fully re-equilibrate after the Ni-spin procedure, the maximum amount of WT<sub>3</sub> trimers that could possibly be present could not account for the observed activity. For example, if we consider the sample enriched for WT<sub>1</sub>MUT<sub>2</sub> trimers (Figure 7b), the maximum fraction of WT<sub>3</sub> trimers that could be present is 0.037, assuming a 2:1 ratio of WT to K131A subunits in the elution. However, even this theoretically maximum amount of WT<sub>3</sub> trimers present could only account for 37% of the activity that was observed in the reaction. On the basis of all of these considerations, we conclude that  $\lambda$ exo trimers containing at least one mutant subunit are active.

## DISCUSSION

At a minimum, the data presented in this study strongly support the conclusion that  $\lambda$ exo does not use a strictly sequential mechanism in which the DNA *must* move from one subunit to the next around the trimer for cleavage to proceed. The Ni-spin pull-down experiments of Figure 4 show that subunit exchange is fully equilibrated after incubation for 1 h at 37 °C. The fact that the material eluted from the Ni-spin column in these experiments contains approximately equal amounts of 6xHis-K131 and untagged WT proteins indicates

that the expected 1:3:3:1 distribution trimer species was formed. The mutant poisoning curve in Figure 6 clearly shows that the exonuclease activity observed at each fraction of K131A mutant is significantly higher than what would be expected for a strictly sequential mechanism and is most consistent with the independent subunits model. Finally, the data in Figure 7 establish that trimers containing at least one mutant subunit are active. All together, the data strongly suggest that  $\lambda$ exo does not use a strictly sequential mechanism of action.

The data also show that trimers containing at least one mutant subunit are not as active as fully WT trimers. The mutant poisoning curve of Figure 6 shows that the observed rates at each fraction of mutant are significantly lower than what would be expected for the WT dominant model, in which trimers containing at least one WT subunit have the full activity of WT<sub>3</sub> trimers. This indicates that during the digestion of a long dsDNA by a hybrid trimer, the DNA does not simply lock on to the active site of a WT subunit for all subsequent rounds of cleavage. If it did, we would expect trimers containing at least one WT subunit to be nearly as active as fully WT trimers.

How do the mutant subunits of hybrid trimers exert their (negative) effect on WT subunits? The data in Figures 6 and 7 are consistent with a model in which the DNA locks onto a single active site on the trimer for multiple rounds of cleavage, but occasionally slips and rebinds to one of the other subunits. If that subunit is WT, processive digestion can resume, with the new active site carrying out further multiple rounds of cleavage. If the subunit is mutant, the trimer will stall on the DNA for a given period of time, until the DNA can rebind to a WT subunit. In this scenario, the rate observed for a given species of trimer would depend on the average rate of the cleavage cycle when the DNA is being digested by a WT subunit, the average number of cleavage events that result from the binding of the DNA to a WT subunit, and the average time it takes the DNA to rebind to an active subunit after a slippage event. This last parameter, the time for rebinding, would depend on the amount of time the DNA spent bound to an inactive subunit, as well as the time it takes to find a new subunit to bind to, be it WT or mutant.

According to this model, a trimer with two mutant subunits would be expected to have a slower rate than a trimer with one mutant subunit, if the time required for the DNA to rebind to a WT subunit after a slippage event is significant relative to the rate of the cleavage cycle. This is because the presence of two mutant subunits on a trimer, as opposed to just one, would increase the amount of time required for the DNA to find an active subunit. The fitted values of 0.56 and 0.12 for  $V_1$  and  $V_2$  shown in Figure 6, which correspond to the rates of WT<sub>2</sub>MUT<sub>1</sub> and WT<sub>1</sub>MUT<sub>2</sub> trimers, respectively, suggest that this is likely to be the case. That these values are lower than the values of 0.66 and 0.33 expected for the independent subunits model likely arises because the amount of time the DNA spends bound to an inactive subunit is significant. The longer it takes the DNA to find an active subunit after a slippage event, the slower the observed rate will be. The average number of slippage events during the digestion of the 2.7 kB dsDNA substrate, and the length of time required for rebinding after slippage, cannot be determined from the present data, but these two parameters would be inversely related to one another, for a given measured rate.

It is interesting to note that the presence of a mutant subunit within a trimer does not appear to diminish processivity. Both for reactions using the hybrid trimer mixtures that were not

subjected to Ni-spin purification (Figure 6), and reactions using the Ni-spin purified material that is devoid of WT<sub>3</sub> trimers (Figure 7), the disappearance of the band for dsDNA substrate is accompanied by the appearance of a band for ssDNA product, with no evidence of intermediate bands. Since the reactions are performed with an excess of DNA substrate over enzyme, the absence of intermediate bands corresponding to partially digested substrates indicates that the reactions are processive. The fact that hybrid trimers retain processivity means that they are still able to hold onto the DNA substrate after a slippage event, presumably due to the threading of the 3'-strand through the central hole on the trimer.

An alternative model to account for how the presence of mutant subunits could reduce the activity of WT subunits is that the mutant subunits could bind to and block the dsDNA ends from being accessed. If the lifetime of the complex of the mutant subunits on the DNA was significantly greater than the rate of the cleavage cycle, then one would expect to observe a decrease in the rate observed for the overall reaction. We consider this explanation unlikely, for several reasons. First, in the experiment of Figure 3, the presence of even a 3-fold excess of K131A mutant (added without prior mixing and subunit exchange) had no effect on the rate observed for fully WT trimers. Second, since the dsDNA substrate is present in large excess over enzyme in the reaction, the great majority of dsDNA ends would be accessible to WT subunits, even if the mutant subunits were to remain bound indefinitely. Third, all of the molecules of DNA were digested in the experiment of Figure 3, indicating that none of the ends were blocked completely, even by a 3-fold excess of K131A mutant. Finally, the gel-shift experiment of Figure 2a shows that the K131A protein binds to dsDNA ends with slightly decreased affinity compared to WT, as opposed to substantially increased affinity. On the basis of all of these considerations, we consider an end-blocking type of mechanism for inhibition unlikely.

Single molecule experiments of  $\lambda$ exo using fluorescence resonance energy transfer (FRET) to measure the rate of digestion of short (~60 bp) dsDNA substrates revealed three phases of the reaction: a initiation phase, in which the enzyme binds to the end of the DNA from bulk solution to initiate digestion, a distributive degradation phase, in which the enzyme begins digesting the DNA but can dissociate after each round of cleavage, and a processive degradation phase, in which the enzyme remains fully engaged with the DNA, digesting it at a more or less constant forward rate.<sup>47</sup> The distributive phase was found to last for about the first ~20 bp of the DNA, after which the processive phase ensued. The transition is likely to occur when the 3'-overhang of the DNA substrate is long enough for the  $\lambda$ exo trimer to remain stably tethered.

Within the context of this experimental framework, it is of interest to ask, at which of the three phases could the mutant subunits be exerting their negative effect? In the single molecule FRET experiments, the rate of digestion for the processive phase was 18 nucleotides per second and was independent of enzyme concentration. At this rate, a 2686 bp DNA like the one used in our study would be completely digested in 149 s. The length of time for the distributive phase ranged from 1 to 200 s and was dependent on  $\lambda$ exo concentration, which ranged from 0.2–60 nM trimer. The concentration of enzyme used in our experiments, 0.05 nM trimer, is four times lower than the lowest concentration used in the single molecule FRET experiment. Thus, the distributive phase would likely be >200 s at the concentration of enzyme used in our study, and the

time required to digest the first 20 bp of the DNA in the distributive phase would on average be greater than the time required to digest the remaining ~2660 bp in the processive phase. By this reasoning, the mutant subunits could conceivably be exerting their negative effect during the distributive phase of the reaction, when the trimers are coming on and off the DNA, instead of during the processive phase of the reaction, as indicated above in our “slippage” model.

However, a potential problem with this line of reasoning is apparent when one considers the experiment of Figure 3, in which the presence of a 3-fold excess of K131A protein had no effect on the rate observed for a fixed concentration of WT. If the mutant subunits had exerted their effect during the distributive phase of the reaction, when the enzyme was coming on and off the DNA, then one would have expected the 3-fold excess of K131A to decrease the rate of the reaction significantly. The fact that an excess of K131A trimers had no effect on the rate of the reaction of WT trimers suggests that either the mutant subunits do not affect the distributive phase of the reaction, or that the distributive phase occurs much more rapidly in solution, where the molecules are free to fully diffuse and tumble in three dimensions, than in the single molecule experiment, where the DNA is tethered to a surface. On the basis of all of these considerations, we consider it likely that the mutant subunits are affecting the processive phase of the reaction, by a mechanism such as that described above in our “slippage” model. Studies of hybrid trimers by single molecule FRET could shed further light on these questions.

## ■ ASSOCIATED CONTENT

### Supporting Information

Figures showing the structure of the  $\lambda$ exo trimer bound to DNA, additional data for the DNA binding assay, and additional data for the mass spectrometry analysis. This material is available free of charge via the Internet at <http://pubs.acs.org>.

## ■ AUTHOR INFORMATION

### Corresponding Author

\*E-mail: bell.489@osu.edu. Telephone: 614-688-3115.

### Funding

This work was funded by Grants MCB-1021966 (to C.E.B.) and DBI-0923551 (to V.H.W.) from the National Science Foundation.

### Notes

The authors declare no competing financial interest.

## ■ ABBREVIATIONS

$\lambda$ exo,  $\lambda$  exonuclease; dsDNA, double-stranded DNA; ssDNA, single-stranded DNA; KB, kilobase; SDS-PAGE, sodium dodecyl sulfate polyacrylamide gel electrophoresis; EDTA, ethylene diamine tetraacetic acid; kDa, kilodaltons; TAE, tris-acetate-EDTA; TBE, tris-borate-EDTA

## ■ REFERENCES

- (1) Kuzminov, A. (1999) Recombinational repair of DNA damage in *Escherichia coli* and bacteriophage lambda. *Microbiol. Mol. Biol. Rev.* **63**, 751–813.
- (2) Stahl, M. M., Thomason, L., Poteete, A. R., Tarkowski, T., Kuzminov, A., and Stahl, F. W. (1997) Annealing vs. invasion in phage  $\lambda$  recombination. *Genetics* **147**, 961–977.
- (3) Little, J. W. (1967) An exonuclease induced by bacteriophage lambda II. Nature of the enzymatic reaction. *J. Biol. Chem.* **242**, 679–686.
- (4) Carter, D. M., and Radding, C. M. (1971) The role of exonuclease and b protein of phage  $\lambda$  in genetic recombination. II. Substrate specificity and the mode of action of  $\lambda$  exonuclease. *J. Biol. Chem.* **246**, 2502–2512.
- (5) Muniyappa, K., and Radding, C. M. (1986) The homologous recombination system of phage lambda. Pairing activities of beta protein. *J. Biol. Chem.* **261**, 7472–7478.
- (6) Vellani, T. S., and Myers, R. S. (2003) Bacteriophage SP1 Chu is an alkaline exonuclease in the SynExo family of viral two-component recombinases. *J. Bacteriol.* **185**, 2465–2474.
- (7) Datta, S., Constantino, N., Zhou, X., and Court, D. L. (2008) Identification and analysis of recombineering functions from Gram-negative and Gram-positive bacteria and their phages. *Proc. Natl. Acad. Sci. U. S. A.* **105**, 1626–1631.
- (8) Kolodner, R., Hall, S. D., and Luisi-DeLuca, C. (1994) Homologous pairing proteins encoded by the *Escherichia coli* recE and recT genes. *Mol. Microbiol.* **11**, 23–30.
- (9) Poteete, A. R. (2001) What makes the bacteriophage lambda Red system useful for genetic engineering: molecular mechanism and biological function. *FEMS Microbiol. Lett.* **201**, 9–14.
- (10) Zhang, Y., Buchholz, F., Muylers, J. P., and Stewart, A. F. (1998) A new logic for DNA engineering using recombination in *Escherichia coli*. *Nat. Genet.* **20**, 123–128.
- (11) Copeland, N. G., Jenkins, N. A., and Court, D. L. (2001) Recombineering: a powerful new tool for mouse functional genomics. *Nat. Rev. Genet.* **2**, 769–779.
- (12) Sharan, S. K., Thomason, L. C., Kuznetsov, S. G., and Court, D. L. (2009) Recombineering: a homologous recombination-based method of genetic engineering. *Nat. Protoc.* **4**, 206–223.
- (13) Wang, H. H., Isaacs, F. J., Carr, P. A., Sun, Z. Z., Xu, G., Forest, C. R., and Church, G. M. (2009) Programming cells by multiplex genome engineering and accelerated evolution. *Nature* **460**, 894–898.
- (14) Rhee, H. S., and Pugh, B. F. (2011) Comprehensive genome-wide protein-DNA interactions detected at single-nucleotide resolution. *Cell* **147**, 1408–1419.
- (15) Clarke, J., Wu, H. C., Jayasinghe, L., Patel, A., Reid, S., and Bayley, H. (2009) Continuous base identification for single-molecule nanopore DNA sequencing. *Nat. Nanotechnol.* **4**, 265–270.
- (16) Lim, B. N., Choong, Y. S., Ismail, A., Glöckler, J., Konthur, Z., and Lim, T. S. (2012) Directed evolution of nucleotide-based libraries using lambda exonuclease. *Biotechniques* **53**, 357–364.
- (17) Kato, M., and Hanyu, Y. (2013) Construction of an scFv library by enzymatic assembly of V(L) and V(H) genes. *J. Immunol. Methods* **396**, 15–22.
- (18) Gerasimova, Y. V., and Kolpashchikov, D. M. (2014) Enzyme-assisted target recycling (EATR) for nucleic acid detection. *Chem. Soc. Rev.* **43**, 6405–6438.
- (19) Liu, L., Lei, J., Gao, F., and Ju, H. (2013) A DNA machine for sensitive and homogeneous DNA detection via lambda exonuclease assisted amplification. *Talanta* **115**, 819–822.
- (20) Zhang, J., Tao, M., and Jin, Y. (2014) An enzyme-aided amplification strategy for sensitive detection of DNA utilizing graphene oxide (GO) as a fluorescence quencher. *Analyst* **139**, 3455–3459.
- (21) Schweighardt, A. J., Battaglia, A., and Wallace, M. M. (2014) Detection of anthrax and other pathogens using a unique liquid array technology. *J. Forensic Sci.* **59**, 15–33.
- (22) Duan, R., Zuo, X., Wang, S., Quan, X., Chen, D., Chen, Z., Jiang, L., Fan, C., and Xia, F. (2014) Quadratic isothermal amplification for the detection of microRNA. *Nat. Protoc.* **9**, 597–607.
- (23) Yuan, Z., Zhou, Y., Gao, S., Cheng, Y., and Li, Z. (2014) Homogenous and sensitive detection of microRNA with ligase chain reaction and lambda exonuclease-assisted cationic conjugated polymer biosensing. *ACS Appl. Mater. Interfaces* **6**, 6181–6185.
- (24) Ge, J., Tang, L. J., Xi, Q., Li, X. P., Yu, R. Q., Jiang, J. H., and Chu, X. (2014) A WS2 nanosheet based sensing platform for highly

- sensitive detection of T4 polynucleotide kinase and its inhibitors. *Nanoscale* 6, 6866–6872.
- (25) Hou, T., Wang, X., Liu, X., Lu, T., Liu, S., and Li, F. (2014) Amplified detection of T4 polynucleotide kinase activity by the coupled 1 exonuclease cleavage reaction and catalytic assembly of molecular beacons. *Anal. Chem.* 86, 884–890.
- (26) Miao, P., Ning, L., Li, X., Shu, Y., and Li, G. (2011) An electrochemical alkaline phosphatase biosensor fabricated with two DNA probes coupled with  $\lambda$  exonuclease. *Biosens. Bioelectron.* 27, 178–182.
- (27) Wang, L., Liu, Y., and Li, J. (2014) Self-phosphorylating deoxyribozyme initiated cascade enzymatic amplification for guanosine-S'-triphosphate detection. *Anal. Chem.* 86, 7907–7912.
- (28) Wang, Y., Chen, J., Jiao, H., Chen, Y., Li, W., Zhang, Q., and Yu, C. (2013) Polymer-templated perylene-probe noncovalent self-assembly: a new strategy for label-free ultrasensitive fluorescence turn-on biosensing. *Chemistry* 19, 12846–12852.
- (29) Kovall, R., and Matthews, B. W. (1997) Toroidal structure of lambda-exonuclease. *Science* 277, 1824–1827.
- (30) Kovall, R. A., and Matthews, B. W. (1999) Type II restriction endonucleases: structural, functional, and evolutionary relationships. *Curr. Opin. Chem. Biol.* 3, 578–583.
- (31) Pingoud, A., Fuxreiter, M., Pingoud, V., and Wende, W. (2005) Type II restriction endonucleases: structure and mechanism. *Cell. Mol. Life Sci.* 62, 685–707.
- (32) Steczkiewicz, K., Muszewska, A., Knizewski, L., Rychlewski, L., and Krzysztof, G. (2012) Sequence, structure and functional diversity of PD-(D/E)XK phosphodiesterase superfamily. *Nucleic Acids Res.* 40, 7016–7045.
- (33) Zhang, J., Xing, X., Herr, A. B., and Bell, C. E. (2009) Crystal structure of *E. coli* RecE protein reveals a toroidal tetramer for processing double-stranded DNA breaks. *Structure* 17, 690–702.
- (34) Zhang, J., McCabe, K. A., and Bell, C. E. (2011) Crystal structures of lambda exonuclease in complex with DNA suggest an electrostatic ratchet mechanism for processivity. *Proc. Natl. Acad. Sci. U.S.A.* 108, 11872–11877.
- (35) Subramanian, K., Rutvisuttinunt, W., Scott, W., and Myers, R. S. (2003) The enzymatic basis of processivity in lambda exonuclease. *Nucleic Acids Res.* 31, 1585–1596.
- (36) Adelman, J. L., Jeong, Y. J., Liao, J. C., Patel, G., Kim, D. E., Oster, G., and Patel, S. S. (2006) Mechanochemistry of transcription termination factor Rho. *Mol. Cell* 22, 611–621.
- (37) Crampton, D. J., Mukherjee, S., and Richardson, C. C. (2006) DNA-induced switch from independent to sequential dTTP hydrolysis in the bacteriophage T7 DNA helicase. *Mol. Cell* 21, 165–174.
- (38) Ariga, T., Muneyuki, E., and Yoshida, M. (2007) F<sub>1</sub>-ATPase rotates by an asymmetric, sequential mechanism using all three catalytic subunits. *Nat. Struct. Mol. Biol.* 14, 841–846.
- (39) Zhou, M., Dagan, S., and Wysocki, V. H. (2012) Protein subunits released by surface collisions of noncovalent complexes: nativelike compact structures revealed by ion mobility mass spectrometry. *Agnew Chem. Int. Ed.* 51, 4336–4339.
- (40) Martin, A., Baker, T. A., and Sauer, R. T. (2005) Rebuilt AAA+ motors reveal operating principles for ATP-fuelled machines. *Nature* 437, 1115–1120.
- (41) Garr, G. W., Furtak, K., Rowland, M. B., Ranson, N. A., Saibil, H. R., Kirchhause, T., and Horwich, A. L. (2000) Multivalent binding of nonnative substrate proteins by the chaperonin GroEL. *Cell* 100, 561–573.
- (42) Nojima, T., Murayama, S., Yoshida, M., and Motojima, F. (2008) Determination of the number of active GroES subunits in the fused heptamer GroES required for interactions with GroEL. *J. Biol. Chem.* 283, 18385–18392.
- (43) Mitsis, P. G., and Kwagh, J. G. (1999) Characterization of the interaction of lambda exonuclease with the ends of DNA. *Nucleic Acids Res.* 27, 3057–3063.
- (44) Dapprich, J. (1999) Single-molecule DNA digestion by lambda-exonuclease. *Cytometry* 36, 163–168.
- (45) Van Oijen, A. M., Blainey, P. C., Crampton, D. J., Richardson, C. C., Ellenberger, T., and Xie, X. S. (2003) Single-molecule kinetics of  $\lambda$  exonuclease reveal a base dependence and dynamic disorder. *Science* 301, 1235–1238.
- (46) Perkins, T. T., Dalal, R. V., Mitsis, P. G., and Block, S. M. (2003) Sequence-dependent pausing of single lambda exonuclease molecules. *Science* 301, 1914–1918.
- (47) Lee, G., Yoo, J., Leslie, B. J., and Ha, T. (2011) Single-molecule analysis reveals three phases of DNA degradation by an exonuclease. *Nat. Chem. Biol.* 7, 367–374.
- (48) Matsuura, S., Komatsu, J., Hirano, K., Yasuda, H., Takashima, K., Katsura, S., and Mizuno, A. (2001) Real-time observation of a single DNA digestion by  $\lambda$  exonuclease under a fluorescence microscope field. *Nucleic Acids Res.* 29, E79.
- (49) Oliver-Calixte, N. J., Uba, F. I., Battle, K. N., Weerakoon-Ratnayake, K. M., and Soper, R. A. (2014) Immobilization of lambda exonuclease onto polymer micropillar arrays for solid-phase digestion of dsDNAs. *Anal. Chem.* 86, 4447–4454.
- (50) Kang, S. H., Lee, S., and Yeung, E. S. (2010) Digestion of individual DNA molecules by  $\lambda$ -exonuclease at liquid-solid interface. *Analyst* 135, 1759–1764.
- (51) Lee, S., Kang, S. H., and Yeung, E. S. (2011) Enzyme digestion of entrapped single-DNA molecules in nanopores. *Talanta* 85, 2135–2141.
- (52) Lee, S., and Kang, S. H. (2013) Single-molecule DNA digestion in various alkanethiol-functionalized gold nanopores. *Talanta* 107, 297–303.